Behavior of poly(d,l-lactic-co-glycolic acid) (PLGA)-based droplets falling into a complex extraction medium simulating the prilling process

Thao-Quyen Nguyen-Pham, Lazhar Benyahia, Guillaume Bastiat, Jeremie Riou, Marie-Claire Venier-Julienne

Version of Record: https://www.sciencedirect.com/science/article/pii/S0021979719313906
Manuscript_7c0a6534452f9d8849a4524d74685dff

Behavior of poly(D,L-lactic-co-glycolic acid) (PLGA) - based droplets falling into a complex extraction medium simulating the prilling process

Nguyen-Pham Thao-Quyen[a], Benyahia Lazhar[b], Bastiat Guillaume[a], Riou Jérémie [a], Venier-Julienne Marie-Claire[a, *]

[a] Micro et Nanomedecines Translationnelles, MINT, UNIV Angers, UMR INSERM 1066, UMR CNRS 6021, Angers, France

[b] Institut des Molécules et des Matériaux du Mans, IMMM, UNIV Le Mans, UMR CNRS 6283, Le Mans, France

[*] Corresponding author at: 4 rue Larrey, 49933 Angers cedex 9, France. Tel: +33628072446. Fax: +33244688546.

E-mail address: marie-claire.venier@univ-angers.fr (M-C. Venier-Julienne)

Abstract

Hypothesis

Prilling process is one of advanced techniques for manufacturing microspheres of controlled and uniform size. In this process, homogenous polymer droplets fall into an extraction medium. The aim of this study was to identify the key parameters influencing the behavior of PLGA polymer-based droplets falling into a complex extraction medium, to select appropriate conditions for prilling.

Experiments

Polymer solutions and extraction media were characterized by determining their viscosity, density and surface tension. A simple model simulating the prilling process was developed to study droplet behavior. Particle shape and velocity at the air-liquid interface and during sedimentation in the container were analyzed step by step. The correlations between the variables studied were visualized by principal component analysis (PCA).

Findings

Droplet deformation at the interface greatly affected the recovery and final particle shape. It depended on the viscosity ratio of polymer solution/extraction medium. The particle shape recovery depended on the viscosity and density of extraction media and polymer solutions. The solidification speed is also an important parameter. In media which the solvent diffused slowly, particles were able to relax and recover their shape, however, they can also deform during sedimentation and collision with the bottom of the cuvette.

Keywords: prilling, PLGA, model, droplet, microsphere.

1. Introduction

Microspheres of biodegradable polymers have many applications for drug delivery [1,2]. Microsphere size, between 1 and 1000 µm, directly influences drug release and the dosage form for a particular route of administration. The critical quality attributes of the drug product therefore depend on the precise control of microsphere size. Diverse techniques are used to produce biodegradable microspheres, including phase separation (coacervation), single or double emulsion/evaporation processes (oil-in-water or water-in-oil-in-water), spray-drying, supercritical CO_2, coaxial electrospray, microfluidics, and hydrogel templates [3,4]. Phase separation, double emulsion and spraying are the techniques most widely used in research and in the manufacturer of marketed drug products [5]. However, these techniques are limited by the lack of uniformity of microsphere size.

Several techniques for the manufacture of microspheres of controlled, uniform size have been developed in recent years [6–8]. Laminar jet breakup (known as prilling) is such an advanced technique considered promising for application from the laboratory to industrial scales [9,10]. In the prilling process, a jet of polymer solution extruded from a nozzle is broken into uniform droplets by a longitudinal vibration. The resulting microdroplets can be solidified by various methods. For example, they can be dropped into an extraction medium in which they are solidified by solvent diffusion [11] or they can be solidified by the ionotropic gelation reaction [12–14]. The behavior of the polymer droplets on impact with the extraction medium surface and during their sedimentation in the medium greatly affects microsphere formation. The observation of these phenomena can help us to identify the critical parameters and to select the most appropriate conditions for prilling.

The phenomena occurring when a falling droplet hits the surface of a liquid have been studied for more than a century (since Reynolds, 1875). Initially, most studies focused on droplets of identical composition to the receiving liquid. When a droplet falls into a deep pool of the same liquid, coalescence or splashing phenomena may occur at the air-liquid interface [15]. In some cases, droplets may also float or bounce on the liquid surface [16]. The transition between bouncing, coalescence and splashing depends principally on droplet diameter, impact velocity, and the density and surface tension of the droplet [17,18]. Several recent studies have considered droplets falling into a liquid with a different composition. Sostarecz and Belmonte (2003), and Mukherjee and Sarkar (2011) reported that a

viscoelastic droplet falling through an immiscible viscous Newtonian medium deformed into a dimpled droplet shape [19,20].

In manufacturing processes for microspheres based on prilling, the droplet is a complex solution of one or two polymers and a mixture of organic solvents. The receiving liquid (the extraction medium) may also be a complex mixture of polymer non-solvents. The choice of polymer solution and extraction medium must allow solvent diffusion to occur. The behavior of the droplets in this process is more complex than that for simple fluids. However, the behavior of a viscoelastic droplet falling into a miscible viscous fluid has never been studied, particularly for the situation in which both are complex fluids.

The aim of this work was to investigate the behavior of poly(D,L-lactic-co-glycolic acid) (PLGA) droplets falling into an extraction medium. Prilling processes involve too high a droplet velocity and too small a droplet size for the observation of droplet behavior during and after impact. We therefore developed a simplified model simulating the prilling process. The organic solvents were chosen on the basis of polymer solubility. The most frequently used solvent in PLGA-based microsphere manufacturing is methylene chloride. However, this molecule is listed in Class 2 of the ICH solvent classification [21], and the limitation of its use is recommended, due to its inherent toxicity. In this study, we used only Class 3 solvents, which are considered to pose no hazard to human health at the levels normally considered acceptable in pharmaceutical products. The characteristics of the polymer solutions, the initial droplets and the extraction media were determined. Within the extraction medium solvent exchange occurs, leading to the solidification of the droplet into a particle. The shape and velocity of the droplets and the particles were recorded, from the air-liquid interface to the bottom of the container. The correlations between different variables were investigated statistically by the principal component analysis.

2. Materials and Methods

2.1. Materials

Poly(D,L-lactic-co-glycolic acid) (PLGA) 50/50 (Resomer® RG 505), containing 25% D-lactic acid, 25% L-lactic acid and 50% glycolic acid, was obtained from Evonik Nutrition & Care GmbH (Essen, Germany). The M_w of PLGA 50/50 was 71,600 Da, and its dispersity (Đ) was 3.9. Acetone and dimethyl sulfoxide (DMSO) were obtained from Sigma-Aldrich (Saint Quentin Fallavier, France). Ethanol and ethyl acetate were obtained from Fisher Scientific (Loughborough, Leics., UK).

2.2. Methods

2.2.1. Polymer solutions

2.2.1.1. Preparation of polymer solutions

The polymer solutions were prepared at room temperature. PLGA (500 mg, 800 mg or 1,100 mg) was dissolved into 10 mL of organic solvent to form polymer solutions (at concentrations of 50 mg/mL, 80 mg/mL and 110 mg/mL, respectively). The organic solvent used was various mixtures of DMSO, acetone and ethyl acetate. PLGA was first dissolved in DMSO, with gentle magnetic stirring, for 2 hours. The desired amounts of acetone and ethyl acetate were then added and mixed to form a homogeneous solution.

2.2.1.2. Characterization of polymer solutions

Dynamic viscosity was determined using a Kinexus® rheometer (Malvern Panalytical, Worcestershire, UK) with a cone plate geometry (diameter 40 mm, angle 2°) at 20°C. The shear stresses were measured with shear rates ranging from 0.5 to 500 s^{-1}. All the polymer solutions displayed Newtonian behavior, and the absolute viscosities (constant values for the dynamic viscosity, independent from the shear rate) were expressed as the shear stress/shear rate ratio.

Density was estimated by measuring the weight of 1000 µL of polymer solution, with an analytical balance with a sensitivity of 0.01 mg (Mettler Toledo XP105DR, Greifensee, Switzerland). Careful management to minimize evaporation was required, due to the high volatility of the organic solvents. The tip for the Finnpipette® 1000 µL-micropipette (Thermo Fisher Scientific, France) was first weighed and the balance tared to zero with this tip. The tip was then filled with 1,000 µL of polymer solution with the Finnpipette® 1000 µL-micropipette. The tip containing the polymer solution was then weighed to determine the weight of 1000 µL of polymer solution. The Finnpipette® 1000 µL-micropipette has a precision (random error) of ± 2 µL and an accuracy (systematic error) of ± 6 µL.

Surface tension was measured with a drop tensiometer device (Tracker Teclis, Longessaigne, France). The surface tension of the polymer solution was evaluated by determining the interfacial tension of a rising air bubble (4 µL, controlled throughout the experiment) in 4 mL of polymer solution. The interfacial tension between the air bubble and the polymer solution was calculated based on image analysis (the shape of the air bubble) and the Laplace equation.

2.2.2. Extraction media

2.2.2.1. Preparation of extraction media

The extraction media used were combinations of ethyl acetate, ethanol and water. The concentration of ethyl acetate ranged from 0% to 25%, and that of ethanol ranged from 50% to 100%. The constraints applied to define the extraction media and the resulting experimental domain are shown in the ternary diagram (Figure SM1). Ethyl acetate is miscible with ethanol, but immiscible with water (solubility in water at 25°C = 7.7% w/w) [22], so ethyl acetate and ethanol were mixed together first, and water was then added to the mixture.

2.2.2.2. Characterization of the extraction media

The dynamic viscosity, density and viscosity of the extraction media were determined as described above, in section 2.2.1.2, for polymer solutions.

2.2.3. Study of the behavior of polymer droplets falling into the extraction medium

2.2.3.1. Model for the droplet behavior study

A model was developed for studying the behavior of a polymer solution droplet on impact with the extraction medium (Figure 1). A 5 mL glass syringe equipped with a BD Microlance™ 3 needle 30G (Becton, Dickinson and Company Limited, County Louth, Ireland) was filled with 2 mL polymer solution. The needle had an internal diameter of 159 ± 19 µm and an external diameter of 311.2 ± 6.4 µm. The syringe was positioned such that the tip of the needle was 25 mm above the surface of the liquid. Droplets were allowed to fall from the needle into a rectangular cuvette containing the extraction medium. The cuvette was 25 mm wide and the extraction medium was 60 mm deep. The ratio of droplet radius to the distance between the droplet and the cuvette wall was kept below 10, to prevent the walls having an effect on droplet behavior [23].

The experiments were conducted at room temperature. Droplet behavior at the air-liquid interface and within the extraction medium during sedimentation was recorded with a Phantom Miro 110 high-speed camera (Vision Research Inc., New Jersey, USA) at a rate of 3000 frames per second (fps) and a resolution of 1280x440 pixels. Once the particles had reached the bottom of the cuvette, they were left for a further five minutes and were then photographed from the top and side with a digital camera. Videos and images from the high-speed camera and the digital camera were analyzed with Phantom Camera Control and

ImageJ software (Research Services Branch, National Institute of Mental Health, Bethesda, Maryland, USA). The experiments were performed in triplicate.

2.2.3.2. Variables studied during impact

The variables studied are presented in Table SM1. The input variables were the experimental conditions, including the characteristics of the polymer solutions, the extraction media and the initial characteristics of the droplets at the air-liquid interface before impact. The output variables were the attributes of the particles during and after impact. These characteristics included the craters and particle shape at the air-liquid interface, the shape and velocity of the particle during sedimentation and the shape of the particle after it had reached the bottom of the cuvette.

The shape ratio of the particles in the extraction medium was determined as the ratio of particle length (L) to particle width (W). Particles were considered spherical if their shape ratio (L/W) was between 1.00 and 1.05, oblate if this ratio was between 1.06 and 1.99 and flat if it exceeded 2.00.

The particle length ratio after/before touching the cuvette bottom (At.Pre.BOT_Size) was calculated as the ratio of the length of the particle at the bottom of the cuvette to its length immediately before it touched the bottom of the cuvette.

Particle sedimentation velocity (m/s) was calculated as the ratio of the depth of extraction medium in the cuvette (60 mm = 0.06 m) to sedimentation time (s).

2.2.3.3. Statistical analysis

Principal component analysis (PCA) was used to visualize potential correlations between the factors studied within samples [24]. PCA is a method of data reduction in which the high dimensionality of the data is reduced to viewable dimensions, i.e. the Principal Components, representing linear combinations of scale factors accounting for most of the variance of the dataset. PCA aims to group samples into homogeneous groups. The illustrative variables used in this analysis provide these projections with meaning, through assessments of the discriminating potential of principal components according to these qualitative variables.

PCA evaluates correlations between variables (input and output). This analysis was performed with the factominer and factoextra packages of R software (R Foundation, Vienna, Austria) [25]. The number of principal components (axes) to be retained was determined with the Kaiser criteria and a graphical approach. PCA plots of quantitative variables summarize the information provided by the dataset. The contributions of the

variables to the projection plane of interest (defined by two principal component axes) are represented by coordinates, making it possible to draw arrows of different directions and lengths. The coordinates of the variables indicate the contributions of the variables and the correlations between variables and axes. Variables making a greater contribution to the projection plane of interest are displayed as longer arrows. The directions of two arrows, or of an arrow and an axis, indicate the degree of association between them. This association can be positive (same direction and close together), negative (opposite direction) or independent (an angle 90° between them).

All quantitative variables were included in the PCA. The shapes of craters and particles were considered to be illustrative variables and were not, therefore, used in the PCA.

3. Results

3.1. Polymer solution characteristics

The characteristics of the PLGA polymer solutions are shown in Table 1. At a polymer concentration of 110 mg/mL (polymer solutions P1, P2 and P3), the component ratio affected viscosity and density, but did not significantly affect surface tension. Viscosity decreased markedly from 43.24 mPa.s to 33.31 mPa.s and density decreased from 0.975 g/cm^3 to 0.878 g/cm^3, from P1 to P3.

With the same organic solvent ratio, a decrease in polymer concentration from 110 mg/mL to 50 mg/mL (polymer solutions P3, P4 and P5) resulted in a decrease in viscosity from 33.31 mPa.s to 6.66 mPa.s whereas only slight differences in density and surface tension were observed between these solutions (0.878 to 0.857 g/cm^3 and 24.52 to 26.64 mN/m, respectively).

3.2. Extraction medium characteristics

The characteristics of the extraction media depended considerably on the component ratio (Table 2). For an identical percentage of ethyl acetate (25% ethyl acetate in media M1 to M3; 12.5% ethyl acetate for media M4 to M6; no ethyl acetate for media M7 to M9), viscosity, density and surface tension decreased with increasing ethanol content or decreasing water content. Conversely, decreasing the proportion of ethyl acetate (from 25% to 0%) increased extraction medium viscosity, density and surface tension.

3.3. Behavior of the droplets on impact

The initial diameter and velocity of the droplets were measured just before the droplets touched the liquid surface. Mean initial droplet diameter was 1.66 ± 0.05 mm and mean

initial droplet velocity at the interface was 0.624 ± 0.013 m/s. The generic behavior of droplets during and after impact is shown for the polymer solution P3 in Figure 2. The droplet was deformed at the interface, and its penetration created a crater on the liquid surface. Particles tended to recover spherical shape, but some were deformed again during sedimentation, possibly even more strongly, by collision with the bottom of the cuvette. In medium M6 (Figure 2A), the droplet adopted a deformed concave shape, subsequently recovering a flat shape that was conserved until the particle reached the bottom of the cuvette. In medium M5 (Figure 2B), the droplet was deformed into a convex shape, subsequently recovering an oblate shape and then deformed again to form a cubic shape with a tail close to the bottom of the cuvette. In medium M7 (Figure 2C), the droplet was deformed into a teardrop-shaped, subsequently recovering a spherical shape. However, the particle extended out to one side and displayed a second deformation into a tailed spherical shape during sedimentation in the cuvette.

3.3.1. Particle deformation and crater generation

Impact with the surface of the medium induced deformation of the droplet. Initial deformation behavior was similar for the various polymer solutions and extraction media (particles at 7 ms of Figure 2A, 2B and 2C). The deformation of droplets of polymer solution P1 during impact with all media M1 to M9 is similar, as shown in Figure SM2.

The penetration of the droplets into the medium created a crater at the liquid surface. Figure 3 shows the behavior of droplets of polymer solutions P1 to P5 at the interface of extraction media M3, M2, M5, M8 and M7 (the behavior of droplets in all media is shown in Figure SM3 and SM4). On the images of Figure 3, the dark line at the top is the air-liquid interface, the dark V or U shape is the crater generated by the impact. The particles are the transparent areas under the craters. Polymer solution viscosity and density increased from P5 to P1. Extraction medium viscosity, density and surface tension increased from left to right in the figure (from M3 to M7). For each polymer solution, the upper panel (a) shows the craters at their maximum depth, and the lower panel (b) shows the deformed particles after the crater has receded.

In Figure 3, polymer solutions P1, P2 and P3 had the higher polymer concentration (110 mg/mL). With increasing extraction medium viscosity, density and surface tension (from M3 to M7), the craters shifted from a V-shape with sharp pointed base to a U shape, with a round base. Particle deformation also varied, with three types of shape observed: concave,

convex or teardrop-shaped. Particle deformation was more concave at lower extraction medium viscosity, density and surface tension (M3), becoming more convex and eventually teardrop-shaped with increasing extraction medium viscosity, density and surface tension.

Droplet deformation also depended on polymer solution viscosity and density. With the same extraction medium, more viscous polymer solutions deformed into less concave or more convex/teardrop-like shapes than less viscous polymer solutions (Figure 3). For example, in medium M3, the concave deformation intensity of deformed droplets decreased from polymer solution P3 to P1. In medium M2, deformed particles of polymer solution P1 were convex while those of polymer solutions P2 and P3 were concave. Similarly, in media M5 and M8, the convex deformation intensity increased from P3 to P1.

For lower concentration polymer solutions P4 and P5 (80 mg/mL and 50 mg/mL, respectively), the craters were U- or V-shaped (Figure 3). The craters obtained with polymer solutions P4 and P5 were larger than those obtained with 110 mg/mL polymer solutions (P1, P2 and P3). The droplets of polymer solutions P4 and P5 displayed a greater deformation than those of polymer solution P3, which had the same component ratio but a higher concentration and viscosity. The particles of polymer solutions P4 and P5 generally stretched out to form tails, which rose with the craters when the craters receded. The stretched parts could be separated from the particles, as fragments (Figure SM4).

Another phenomenon was observed in extraction medium M7, which had the highest viscosity, density and surface tension. In this medium, the particles of polymer solutions P1, P4 and P5 hung below the air-liquid interface after penetration, whereas those of polymer solutions P2 and P3 detached from the surface and descended into the medium.

Statistical analysis

The particles of the 80 mg/mL and 50 mg/mL polymer solutions (P4 and P5, low viscosity) were mostly shapeless or deformed into fragments during the experiments. They could not, therefore, be used to analyze the correlations between variables. The correlation analysis was therefore based exclusively on the 110 mg/mL polymer solutions P1, P2 and P3. In this analysis, the first two axes accounted for 74% of the total variance of the sample (49.9% for axis 1 and 24% for axis 2). Based on the Kaizer criteria and a graphical approach, these dimensions were retained for studies of the correlation between variables (Figure SM5).

Crater shape and particle shape deformation (illustrative variables) are presented on the PCA plots for individual experiments, with axis 1 and axis 2 (Figure SM5A and SM5B). The

sample codes are indicated in Appendix 1. These experiments formed several separate groups with different properties, making it possible to explain the differences between quantitative variable correlations.

3.3.2. Particle shape recovery

Droplet deformation greatly affected the recovery of particle shape. The relationship between the deformed and recovery shapes is shown in PCA plots of illustrative variables (Figure SM5B and SM5C). Particles that became concave on deformation recovered flat or oblate shapes. Particles that became convex on deformation recovered oblate or spherical shapes and particles that became teardrop-shaped on deformation recovered a spherical shape (Figure 4A and 4B).

The particle shape ratio was defined as the ratio of particle length (L) to width (W), so the particles with a ratio closest to 1 were considered to be the most spherical. The particle recovery shape ratio of samples (Recov_Size) is presented in detail in Figure 5A. Generally, the particle recovery shape ratio (Recov_Size) decreased when increasing the viscosity, density and surface tension of the extraction medium, and it increased from polymer solution P1 to P3.

Correlations between particle recovery shape ratio and extraction medium

In the PCA plot for quantitative variables (Figure SM6), particle recovery shape ratio (Recov_Size) was strongly inversely correlated with the viscosity, density and surface tension of the extraction medium (Vis_M, Dens_M and ST_M, respectively). These findings are consistent with the observations in Table SM2, with a greater recovery of particle shape observed at higher extraction medium viscosity, density and surface tension. An observation of particle shape recovery in extraction media from M3 to M2 showed that concave particles recovered an oblate shape in higher viscosity extraction media, but they remained flat in lower viscosity media (Table SM2). In media M4 and M7, all particles recovered a spherical shape, other than those of polymer solution P1 in medium M7, which hung below the air-liquid interface.

The composition of the extraction medium also influenced particle recovery shape ratio. The percentage of water (X.Water_M) was strongly inversely correlated with particle recovery shape ratio (Recov_Size). By contrast, the percentage of ethanol (X.EtOH_M) was strongly positively correlated with particle recovery shape ratio (Recov_Size). Thus, particle

shape recovery was stronger for higher percentages of water and lower percentages of ethanol.

Correlations between particle recovery shape ratio and polymer solution

Polymer solution viscosity (Vis_P) was not correlated with particle recovery shape ratio (Recov_Size) (90° between them; Figure SM6). This lack of correlation is consistent with the particle deformation behavior observed at the air-liquid interface (section 3.3.1), which was similar for the droplets of polymer solutions P1, P2 and P3. However, the PCA was based exclusively on the dataset for polymer solutions P1, P2 and P3. The small differences in viscosity between polymer solutions P1, P2 and P3 may explain the lack of correlation between polymer solution viscosity and particle recovery shape ratio in the PCA.

By contrast, the polymer solution/extraction medium viscosity ratio (Vis_P.M) was strongly positively correlated with particle recovery shape ratio (Recov_Size), demonstrating that polymer solution viscosity nevertheless influenced particle recovery (Figure SM6). This influence was observed in comparisons of the lower viscosity polymer solutions P4 (15.83 mPa.s) and P5 (6.66 mPa.s) with the higher viscosity polymer solutions P1, P2 and P3 (33.31 – 43.24 mPa.s). In the same extraction medium, the particles of the lower viscosity polymer solutions P4 and P5 recovered their shape with much greater difficulty than those of the higher viscosity polymer solutions P1, P2 and P3 (Figure 3, Figure SM3 and SM4).

Similarly, the particles of polymer solution P1 (higher viscosity) recovered their shape more effectively than those of polymer solutions P2 and P3 (Table SM2). In media M3 to M2, the particles of polymer solution P1 recovered an oblate shape more readily than those of polymer solutions P2 and P3. In addition, in medium M8, only particles of polymer solution P1 were able to recover a spherical shape, those of polymer solutions P2 and P3 being oblate.

As for polymer viscosity, no correlation was observed between the surface tension of the polymer solution (ST_P) and particle recovery shape ratio (Recov_Size). However, the polymer solution/extraction medium surface tension ratio (ST_P.M) and particle recovery shape ratio (Recov_Size) were strongly positively correlated (Figure SM6). The surface tensions of polymer solutions did not differ significantly, so the particle recovery shape ratio was dependent only on the surface tension of the extraction medium.

Neither the density of the polymer solution (Dens_P) nor the polymer solution/extraction medium density ratio (Dens_P.M) was correlated with particle shape ratio (Figure SM6).

3.3.3. Deformation of the particles in the medium

Deformation during particle sedimentation in the medium

While settling out on their way to the bottom of the cuvette, the particles deformed again into various shapes: flat, oblate, cubic, cubic with a tail (cubic-tail) or spherical with a tail (spherical-tail) (Figure 4C). "The tail" was defined as a prolongation of the surface of the particle. The shape of the particles before they touched the bottom of the cuvette (Pre.BOT_Shape) is presented in the PCA plot (Figure SM5D) and in relation to the previous stages (Table SM2 C).

On the PCA plot of quantitative variables (Figure SM6), the shape ratio of particles before they reached the bottom of the cuvette (Pre.BOT_Size) was strongly positively correlated with the particle recovery shape ratio (Recov_Size). Thus, the shape ratio of particles before they reached the bottom of the cuvette (Pre.BOT_Size) was also dependent on extraction medium characteristics (viscosity, density and surface tension), extraction medium components (percentages of water and ethanol) and polymer solution viscosity.

The shape ratio of the particles before they touched the bottom of the cuvette (Pre.BOT_Size) is presented in detail in Figure 5B. The particles in medium M1 were less deformed by sedimentation (no tail) than those of the other media (Table SM2C). Generally, extraction media M5, M1, M8, M4 and M7 gave acceptable levels of deformation, with a deformed shape ratio below 1.33 (Figure 5B). In these media, the shape deformation ratios of polymer solutions P1, P2 and P3 were almost identical.

Particle sedimentation velocity (Vel_Fall) was strongly positively correlated with polymer solution/extraction medium density ratio (Dens_P.M). Vel_Fall was also strongly negatively correlated with extraction medium viscosity (Vis_M) (Figure SM6). This result was consistent with the sedimentation velocity of a sphere falling in a fluid calculated according to Stokes' law (Appendix 2). The sedimentation velocity of the particles in the extraction media was also determined (Figure 6). When the extraction media were ordered according to extraction medium viscosity, density and surface tension (which increased from M3 to M7, as in Figure 6), sedimentation velocity increased from medium M3 to M9 and then decreased to medium M7. This trend was similar to that for the polymer solution/extraction medium density ratio

(data not shown). Particularly for polymer solution P1, sedimentation velocity was much lower in medium M4 than in medium M8. In medium M7, the particles of polymer solution P1 hung below the air-liquid interface.

Deformation by collision with the cuvette bottom

The particle deformation resulting from collision with the bottom of the cuvette depended on the solidification of the particle during settling out. The change in particle shape due to the collision is represented as the particle length ratio after/before touching the bottom of the cuvette (At.Pre.BOT_Size) in Figure 5C. Higher values of this ratio indicate a greater deformation of the particles.

In the extraction media without water (M3, M6 and M9), the particles displayed almost no deformation due to the collision with the bottom of the cuvette (particle length ratio after/before touching (At.Pre.BOT_Size) of about 1). In medium M3, ratios below 1 were even obtained with polymer solutions P1 and P2. The ratios were higher in media M2, M5, M1 and M4. These media contained a high proportion of ethyl acetate: 25% in M1 and M2, 12.5% in M4 and M5. In media without ethyl acetate (M8 and M7), the particle length ratio after/before touching the bottom of the cuvette (At.Pre.BOT_Size) was lower than that in media with ethyl acetate.

In most of the media, particle length ratio after/before touching the bottom of the cuvette (At.Pre.BOT_Size) was lower for polymer solution P3 than for polymer solutions P1 and P2. However, in medium M5, At.Pre.BOT_Size of polymer solution P3 was slightly higher than of polymer solution P2. Besides, in medium M3, At.Pre.BOT_Size of polymer solution P3 was higher than of polymer solution P1 and P2. The ratios of polymer solutions P1 and P2 were very similar, except in media M2 and M5, in which they were much higher for P1 (Figure 5C).

4. Discussion

In the model developed here, the initial deformation of the polymer droplet at the air-liquid interface was a critical point. The resulting particle shape greatly influenced the subsequent behavior of the particle in the medium. At first, only the bottom of the droplet penetrated the air-liquid interface, this initial deformation being similar between samples (Figure SM2). The droplet then continued to descend in the medium, creating a crater at the surface of the medium (Figure 3, SM3 and SM4).

The movement of the particle and the medium induced the deformation of the particle into different shapes (concave, convex or teardrop-shaped). This deformation was caused by three forces acting on the particle: (1) inertia, forcing the particle to descend in the medium, (2) friction between the two viscous liquids, which stretched the particle and (3) particle surface tension, which acts to conserve the spherical shape [19,20,26,27]. The movements of the liquid in the medium and the liquid within the particle are displayed in Figure 7. The liquid within the particle, particularly at its surface, moved with these forces due to the viscoelastic stress. If the friction force was smaller than the viscoelastic stress, the surface of the particle was deflected inwards, generating a concave shape (Figure 7A). Increases in friction force tended to stretch the particles out into a convex (Figure 7B) or teardrop-shaped (Figure 7C).

Crater recession after maximum depth had been reached influenced particle deformation. The craters pulled the top/center of the particles upward during their recession, resulting in a teardrop-shaped or convex particle or in small peaks at the center of concave particles (polymer solution P1, P2 and P3 in Figure 3 and SM3). This effect was most clearly observed with the low-viscosity polymer solutions P4 and P5, in which particles were stretched out to form long tails (Figure 3 and SM4). However, the particle behavior in medium M7 was slightly different from other media. In medium M7, particles were also stretch out, however, they were hung below the air-liquid interface after the craters receded. Particles of polymer solutions P2 and P3 were hung in a short time then detached from the surface and descended into the medium. In contrast, particles of polymer solutions P1, P4 and P5 were hung below the air-liquid interface for more than 5 minutes (observation time of every experiment was 5 minutes).

The polymer solution/extraction medium viscosity ratio (Vis_P.M) was evaluated to investigate the deformation phenomenon (Figure 8). This viscosity ratio (Vis_P.M) decreased from medium M3 to medium M7. It also decreased from P1 to P5. The higher the viscosity ratio, the more viscous the polymer solution relative to the medium, and the smaller the amount of stretching deformation.

Particle shape recovery clearly depended on the viscosity and density of extraction media and polymer solutions. It also depended on particle solidification speed (the rate of diffusion of organic solvents from the particle core to the extraction medium). In media with a high proportion of water and a low proportion of ethanol, the solvent diffused slowly. The

particles remained in the liquid state and were better able to recover/relax. By contrast, in media with a high proportion of ethanol, the deformed particles were more solid, and the recovery of a spherical shape was much more difficult. Specifically, from medium M1 to M2, M3, the water proportion decreased, and the ethanol proportion increased (Table 2), thereby the solvent diffusion rate increased from M1 to M2, M3. Particles in medium M3 were more solid and more difficult to recover their shapes than those in M2 and M1. Consequently, the particle shape recovery ratio in medium M3 was higher than in M2 and M1. In the same way, the particle shape recovery ratio declined from medium M6 to M5 and M4, from M9 to M8 and M7 (Figure 5A).

The redeformation of particles during settling out may be due to the higher pressure deep in the liquid. For drops descending deep into the medium, the pressure of the medium increased according to the following formula: p=g x d x ρ (g is the gravitation acceleration, d is the depth of liquid and ρ is medium density). The difference in equilibrium pressure between the particle and the medium at the interface was due to the interfacial tension (the Young-Laplace equation). As the particles descended, the external pressure increased, causing the internal pressure to increase. When the pressure exceeded the equilibrium limit of the interfacial tension, the liquid escaped from the particle to the medium, initially from the weakest point on the particle surface, forming a “tail” on the particle. Particles recovering oblate or spherical shapes could subsequently undergo further deformation into the cubic-tail or spherical-tail shapes. Liquid leaking from the weakest point of the particle (a tail) was also observed on particles at the bottom of the cuvette (see Figure 2B, for example). Redeformation due to liquid pressure could be decreased by decreasing the depth of extraction medium and by using continuous stirring to prevent particle aggregation and sedimentation. However, shear stress may also influence particle shape, so the shape and size of the container must be taken into account, together with stirring speed.

Another factor influencing redeformation was particle solidification speed. As the amount of the diffused solvent increased, the particles became more solid, and less susceptible to deformation by the pressure of the medium. It was difficult to estimate solvent diffusion in this study due to the complex composition of the polymer solutions and the extraction media. However, solvent diffusion/particle solidification can be evaluated by considering particle deformation due to collision with the bottom of the cuvette, as assessed

by the particle length ratio after/before touching bottom of the cuvette (At.Pre.BOT_Size, Figure 5C).

In general, the droplets of polymer solution P3 had a higher diffused solvent content than those of polymer solutions P1 and P2. This may be due to the percentage of ethyl acetate in polymer solution P3 (12.5%) being lower than that in P1 and P2 (75% and 50%, respectively). Ethyl acetate is not very soluble in water (7.7% at 25°C [22]), so higher concentrations of ethyl acetate may slow solvent diffusion. Furthermore, the density of the polymer solution increased with the increasing ethyl acetate content, resulting in faster sedimentation, with less time for diffusion to occur (Figure 6).

In the extraction media without water (M3, M6 and M9), solvent diffusion was more effective, and the particles were not significantly deformed by collision. In media M6 and M9, the particle length ratios after/before touching the cuvette bottom (At.Pre.BOT_Size) were about 1 (Figure 5C). Medium M3 had a higher concentration of ethyl acetate than M6 and M9, so solvent diffusion was slower, particularly with polymer solutions P1 and P2. The particles of polymer solutions P1 and P2 remained in the liquid state and continued to recover/relax after reaching the bottom of the cuvette. They shrank rather than stretched, so the particle length ratios after/before touching the bottom of the cuvette (At.Pre.BOT_Size) were below 1 (Figure 5C).

Similarly, in extraction media with higher concentrations of ethyl acetate (M2, M5, M1 and M4), more solvent diffusion was observed than in media M8 and M7, displayed by the higher particle length ratios after/before touching the bottom of the cuvette (Figure 5C). Moreover, more solvent diffusion was observed in medium M8 than in medium M7, despite the higher concentration of ethanol. This may be due to the sedimentation velocity of the droplets in medium M8, which was greater than that in medium M7 (Figure 6).

The application of the results of this study to the prilling process will require the difference in initial droplet size between the model and the prilling process to be taken into account. The initial droplet size in the model was 1.66 ± 0.05 mm, with an ideal microsphere size of less than 100 µm [1]. If initial droplet size were to be decreased, the initial deformation of the droplet due to impact with the extraction medium surface might become negligible. In this case, increasing the viscosity ratio of the polymer solution/medium would decrease the stretching effect, resulting in more spherical particles.

Besides, particle recovery was difficult when solvent diffusion was rapid. However, slow solvent diffusion might lead to the redeformation of the recovered particles. A solvent diffusion giving an optimal balance between particle recovery and redeformation must therefore be found. With a small initial droplet size, the microdroplets are less deformed or not deformed at all and may retain their spherical shape after they have penetrated the surface of the medium. In such conditions, faster solvent diffusion is more appropriate.

5. Conclusion

The behavior of droplets in this study is consistent with previous findings about droplet falling into a liquid, which could be splashing, coalescence, bouncing, floating [15–18], noncoalescence [28] or submergence [29] when colliding with the liquid surface, then deforming into fragment [30], dimple shape [19,20], oblate spheroid [31] or recovering into spherical shape [29]. In order to understand the deformation and recovery mechanism, we presented step by step the changes of droplet shape from the air-liquid interface to the recovery phase. The droplets underwent the concave, convex or teardrop-shaped before relaxing and recovering their shapes. Furthermore, the droplet deformation due to sedimentation and collision with the bottom of container were also analyzed. We analysed the most critical parameters influencing the droplet behavior. In previous studies, viscosity ratio and interfacial tension between two fluids were determined as the most important parameters influencing the droplet deformation [32] and droplet relaxation [33]. However, unlike these studies in which droplets and receiving medium were similar or immiscible fluids, the fluids in our study were miscible, complex and polymer-containing fluids. Thus, the interfacial tension was difficult to quantify. The behavior of droplets was determined depending on the polymer solution/extraction medium viscosity ratio, extraction medium properties (viscosity, density), polymer solution properties (viscosity, density) and the solvent diffusion (which related to the liquids' components).

Our results show the importance of studying the behavior of polymer droplets on impact with an extraction medium, because observed phenomena and correlations should facilitate the selection of appropriate organic solvents, extraction media and conditions for microencapsulation process, especially prilling. Droplet size is smaller in prilling process, resulting in a lower impact energy, less deformation and a higher diffusion rate. However, the jet of liquid exerts a very strong force, increasing the initial velocity and impact energy.

The most appropriate values of these parameters should be determined, to ensure the obtainment of spherical microparticles during prilling. This work is currently underway.

Conflicts of interest

The authors have no competing financial interest to declare.

Acknowledgments

We would like to thank Dr. Brice Calvignac for his help and advice concerning the use of the high-speed camera.

References

[1] K.K. Kim, D.W. Pack, Microspheres for Drug Delivery, in: M. Ferrari, A.P. Lee, L.J. Lee (Eds.), BioMEMS and Biomedical Nanotechnology, Springer US, Boston, MA, (2006) 19–50. doi:10.1007/978-0-387-25842-3_2.

[2] F. Qi, J. Wu, H. Li, G. Ma, Recent research and development of PLGA/PLA microspheres/nanoparticles: A review in scientific and industrial aspects, Frontiers of Chemical Science and Engineering. 13 (2019) 14–27. doi:10.1007/s11705-018-1729-4.

[3] F.Y. Han, K.J. Thurecht, A.K. Whittaker, M.T. Smith, Bioerodable PLGA-Based Microparticles for Producing Sustained-Release Drug Formulations and Strategies for Improving Drug Loading, Frontiers in Pharmacology. 7 (2016) 185. doi:10.3389/fphar.2016.00185.

[4] S. Tamilvanan, R.V. Babu, K. Kannan, Manufacturing Techniques and Excipients Used During the Design of Biodegradable Polymer-based Microspheres Containing Therapeutic Peptide/Protein for Parenteral Controlled Drug Delivery, PDA Journal of Pharmaceutical Science and Technology. 62 (2008) 125-154.

[5] A. Schoubben, M. Ricci, S. Giovagnoli, Meeting the unmet: from traditional to cutting-edge techniques for poly lactide and poly lactide-co-glycolide microparticle manufacturing, Journal of Pharmaceutical Investigation. 49 (2019) 381-404. doi:10.1007/s40005-019-00446-y.

[6] Z. Liu, X. Li, B. Xiu, C. Duan, J. Li, X. Zhang, X. Yang, W. Dai, H. Johnson, H. Zhang, X. Feng, A novel and simple preparative method for uniform-sized PLGA microspheres: Preliminary application in antitubercular drug delivery, Colloids and Surfaces B: Biointerfaces. 145 (2016) 679–687. doi:10.1016/j.colsurfb.2016.05.085.

[7] B. Amoyav, O. Benny, Microfluidic Based Fabrication and Characterization of Highly Porous Polymeric Microspheres, Polymers. 11 (2019) 419. doi:10.3390/polym11030419.

[8] Y. Lu, M. Sturek, K. Park, Microparticles produced by the hydrogel template method for sustained drug delivery, International Journal of Pharmaceutics. 461 (2014) 258–269. doi:10.1016/j.ijpharm.2013.11.058.

[9] C. Heinzen, A. Berger, I. Marison, Use of Vibration Technology for Jet Break-Up for Encapsulation of Cells and Liquids in Monodisperse Microcapsules, in: V. Nedović, R. Willaert (Eds.), Fundamentals of Cell Immobilisation Biotechnology, Springer Netherlands, Dordrecht, (2004) 257–275. doi:10.1007/978-94-017-1638-3_14.

[10] T. Sakai, N. Hoshino, Production of uniform droplets by longitudinal vibration of audio frequency, Journal of Chemical Engineering of Japan. 13 (1980) 263–268. doi:10.1252/jcej.13.263.

[11] F. Violet, M.-Q Le., M. Sergent, G. Bastiat, V.-T. Tran, M.-C. Venier-Julienne, Development of prilling process for biodegradable microspheres through experimental designs, International Journal of Pharmaceutics. 498 (2016) 96–109. doi:10.1016/j.ijpharm.2015.11.051.

[12] P. Del Gaudio, G. Auriemma, P. Russo, T. Mencherini, P. Campiglia, M. Stigliani, R.P. Aquino, Novel co-axial prilling technique for the development of core–shell particles as delayed drug delivery systems, European Journal of Pharmaceutics and Biopharmaceutics. 87 (2014) 541–547. doi:10.1016/j.ejpb.2014.02.010.

[13] S.H. Ching, N. Bansal, B. Bhandari, Alginate gel particles–A review of production techniques and physical properties, Critical Reviews in Food Science and Nutrition. 57 (2017) 1133–1152. doi:10.1080/10408398.2014.965773.

[14] G. Auriemma, T. Mencherini, P. Russo, M. Stigliani, R.P. Aquino, P. Del Gaudio, Prilling for the development of multi-particulate colon drug delivery systems: Pectin vs. pectin–alginate beads, Carbohydrate Polymers. 92 (2013) 367–373. doi:10.1016/j.carbpol.2012.09.056.

[15] F. Rodriguez, R. Mesler, Some drops don’t splash, J. Colloid Interface Sci. 106 (1985) 347–352. doi:10.1016/S0021-9797(85)80008-4.

[16] M. Rein, Phenomena of liquid drop impact on solid and liquid surfaces, Fluid Dynamics Research. 12 (1993) 61–93. doi:10.1016/0169-5983(93)90106-K.

[17] M. Rein, The transitional regime between coalescing and splashing drops, Journal of Fluid Mechanics. 306 (1996) 145-165. doi:10.1017/S0022112096001267.

[18] S.L. Zhbankova, A.V. Kolpakov, Collision of water drops with a plane water surface, Fluid Dynamics. 25 (1990) 470–473. doi:10.1007/BF01049832.

[19] M.C. Sostarecz, A. Belmonte, Motion and shape of a viscoelastic drop falling through a viscous fluid, Journal of Fluid Mechanics. 497 (2003) 235–252. doi:10.1017/S0022112003006621.

[20] S. Mukherjee, K. Sarkar, Viscoelastic drop falling through a viscous medium, Physics of Fluids. 23 (2011) 013101. doi:10.1063/1.3533261.

[21] International Council for Harmonisation of Technical Requirements for Pharmaceuticals for Human Use, Q3C(R7) Impurities: Guideline for Residual Solvents, 2016. https://www.ich.org/products/guidelines/quality/quality-single/article/impurities-guideline-for-residual-solvents.html

[22] R.C. Rowe, P.J. Sheskey, M.E. Quinn, Handbook of pharmaceutical excipients, 6. ed, APhA, (PhP) Pharmaceutical Press, London, (2009) 254.

[23] P.C.-H. Chan, L.G. Leal, The motion of a deformable drop in a second-order fluid, Journal of Fluid Mechanics. 92 (1979) 131–170. doi:10.1017/S0022112079000562.

[24] K. Pearson, LIII. On lines and planes of closest fit to systems of points in space, The London, Edinburgh, and Dublin Philosophical Magazine and Journal of Science. 2 (1901) 559–572. doi:10.1080/14786440109462720.

[25] S. Lê, J. Josse, F. Husson, FactoMineR : An R Package for Multivariate Analysis, Journal of Statistical Software. 25 (2008) 1-18. doi:10.18637/jss.v025.i01.

[26] B.Z. Vamerzani, M. Norouzi, B. Firoozabadi, Analytical solution for creeping motion of a viscoelastic drop falling through a Newtonian fluid, Korea-Australia Rheology Journal. 26 (2014) 91–104. doi:10.1007/s13367-014-0010-8.

[27] R.M. Valladares, P. Goldstein, C. Stern, A. Calles, Simulation of the motion of a sphere through a viscous fluid, Revista Mexicana de Física. 49 (2003) 166–174.

[28] M.S. Khan, D. Kannangara, W. Shen, G. Garnier, Isothermal Noncoalescence of Liquid Droplets at the Air−Liquid Interface, Langmuir. 24 (2008) 3199–3204. doi:10.1021/la7028627.

[29] E. Yakhshi-Tafti, H.J. Cho, R. Kumar, Impact of drops on the surface of immiscible liquids, J. Colloid Interface Sci. 350 (2010) 373–376. doi:10.1016/j.jcis.2010.06.029.

[30] S. Residori, P.K. Buah-Bassuah, F.T. Arecchi, Fragmentation instabilities of a drop as it falls in a miscible fluid, Eur. Phys. J. Spec. Top. 146 (2007) 357–374. doi:10.1140/epjst/e2007-00193-8.

[31] T.D. Taylor, A. Acrivos, On the deformation and drag of a falling viscous drop at low Reynolds number, J. Fluid Mech. 18 (1964) 466–476. doi:10.1017/S0022112064000349.

[32] S. Guido, M. Villone, Measurement of Interfacial Tension by Drop Retraction Analysis, J. Colloid Interface Sci. 209 (1999) 247–250. doi:10.1006/jcis.1998.5818.

[33] K. Moran, A. Yeung, J. Masliyah, Shape relaxation of an elongated viscous drop, J. Colloid Interface Sci. 267 (2003) 483–493. doi:10.1016/j.jcis.2003.07.014.

Figures

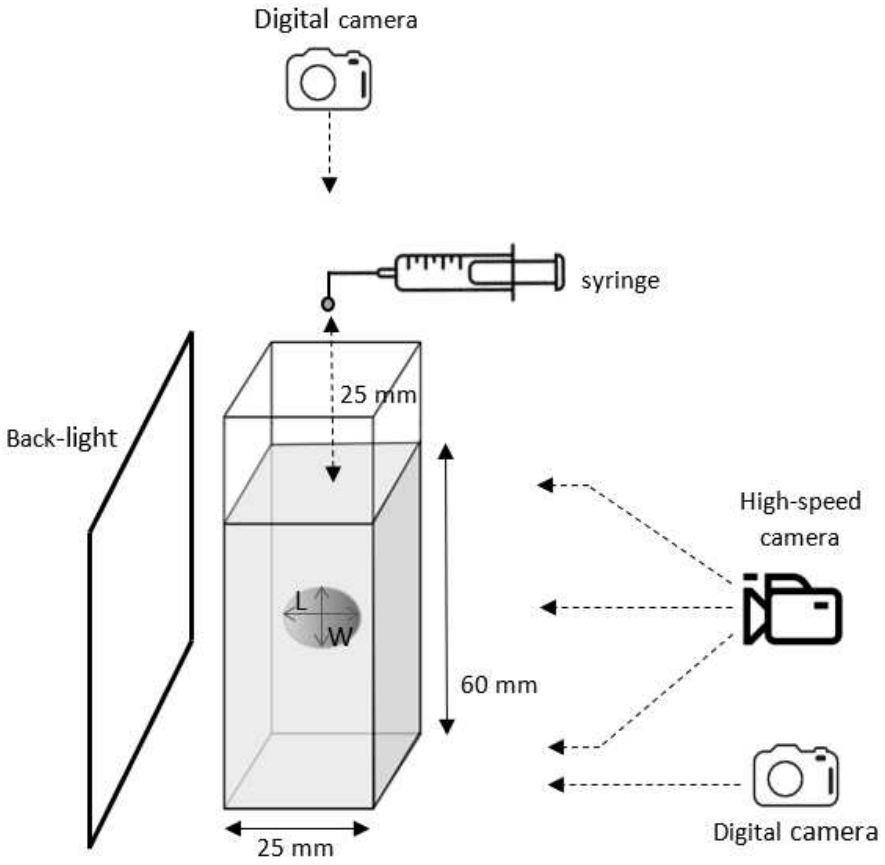

Figure 1. Diagram of the model used to study polymer droplet behavior. L and W are the largest and smallest dimensions of the particle. Particle shape ratio was defined as the ratio L/W.

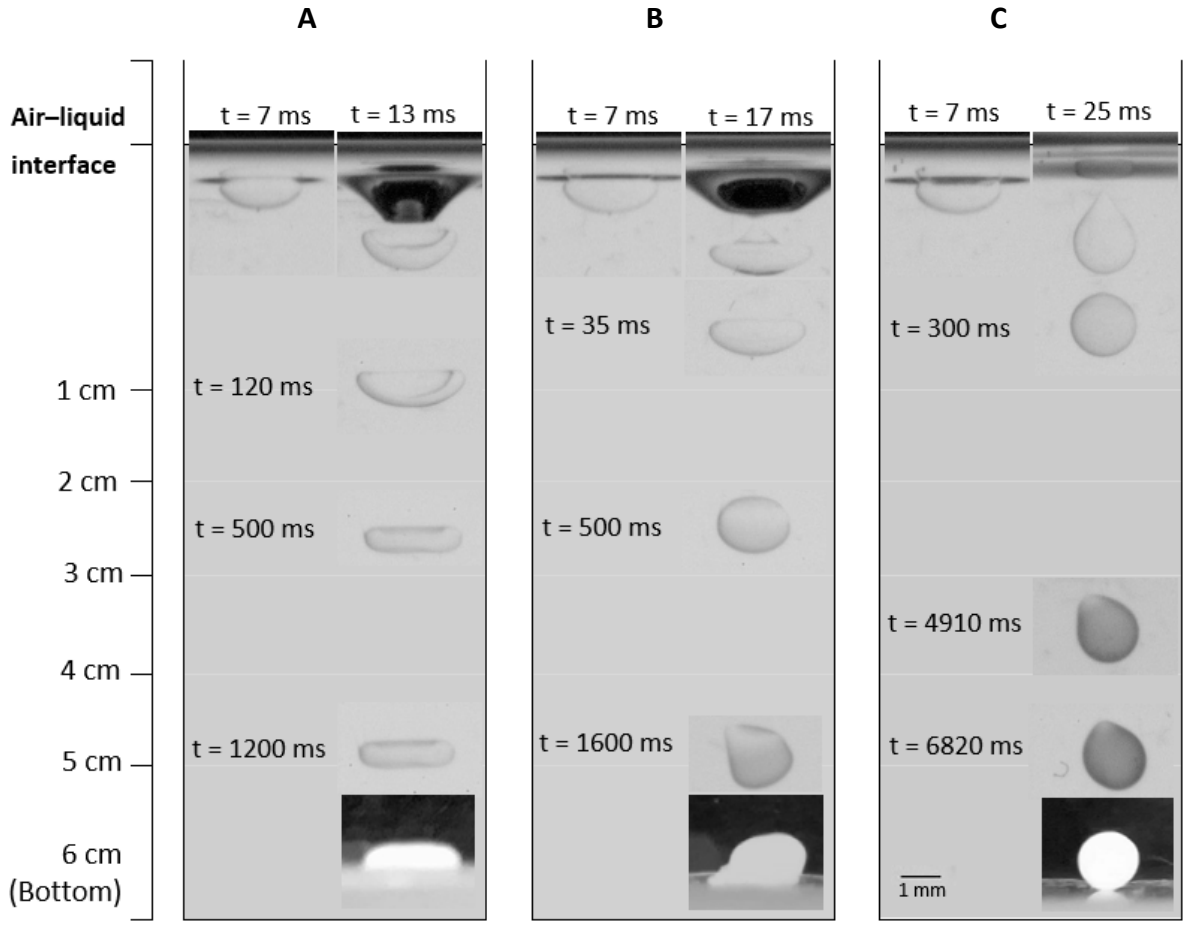

Figure 2. Behavior of droplets of polymer solution P3 (110 mg/mL, DMSO/ethyl acetate/acetone 25/12.5/62.5) during and after impact with extraction media (A) M6 (ethyl acetate/ethanol 12.5/87.5), (B) M5 (ethyl acetate/ethanol/water 12.5/68.75/18.75) and (C) M7 (ethanol/water 50/50). On images at the air-liquid interface, the dark line at the top is the interface and the transparent area under the interface is the deformed particle. The scale on the left indicates the depth of the medium in the cuvette. In different extraction media, droplets deformed, recovered and redeformed into different shapes at different times and depths.

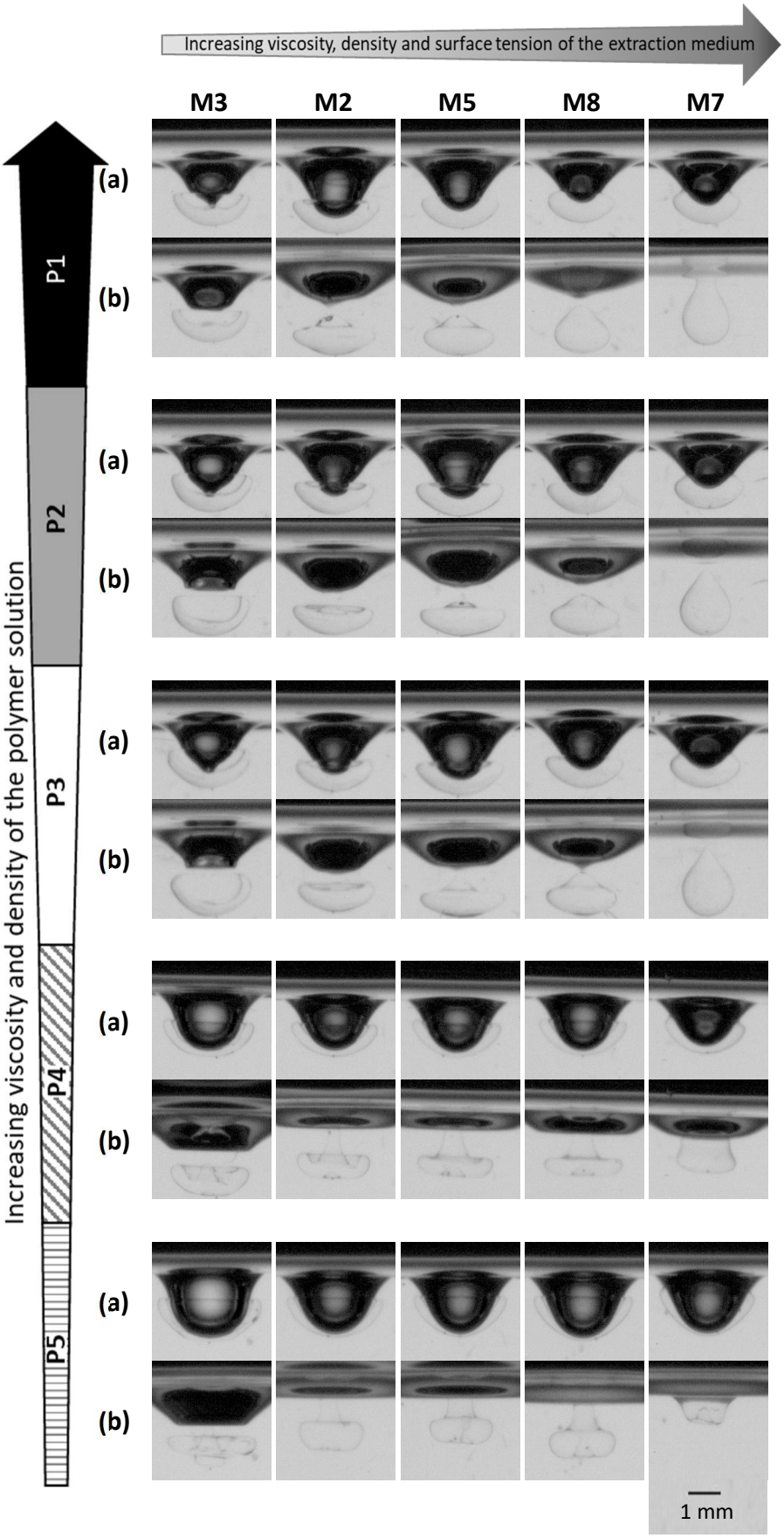

Figure 3. Impact of droplets of polymer solutions P1 to P5 at the air-liquid interface with extraction media. The viscosity and density of the polymer solution increased from P5 to P1. The upper row (a) shows the craters at their maximum depth, before they receded; the lower row (b) shows droplet deformation after the droplet left the crater. In extraction medium M7, particles hung below the air-liquid interface after the craters receded.

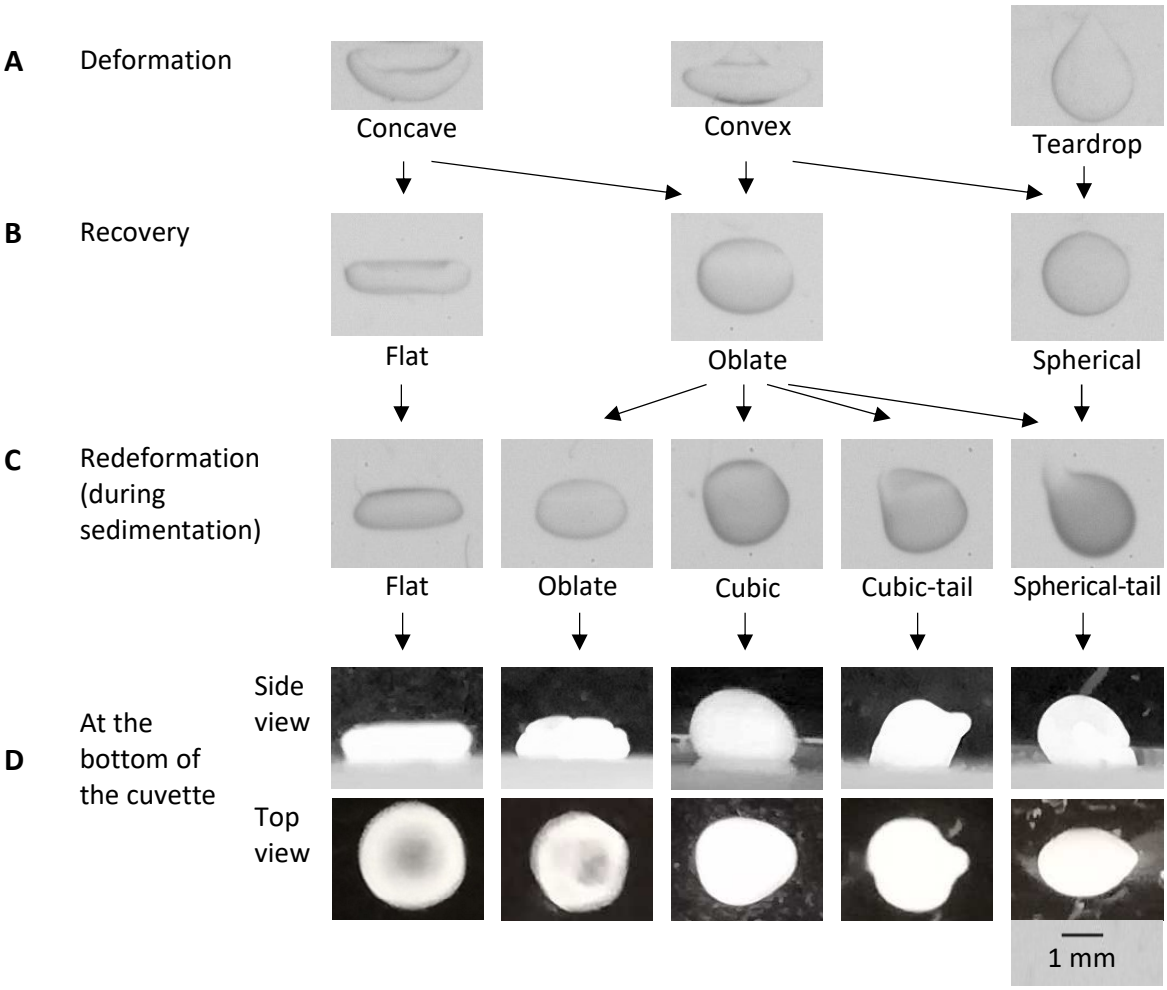

Figure 4. Particle shapes at different stages: (A) deformation at the air-liquid interface, (B) recovery, (C) redeformation during sedimentation, (D) particle after five minutes at the bottom of the cuvette (top and side views).

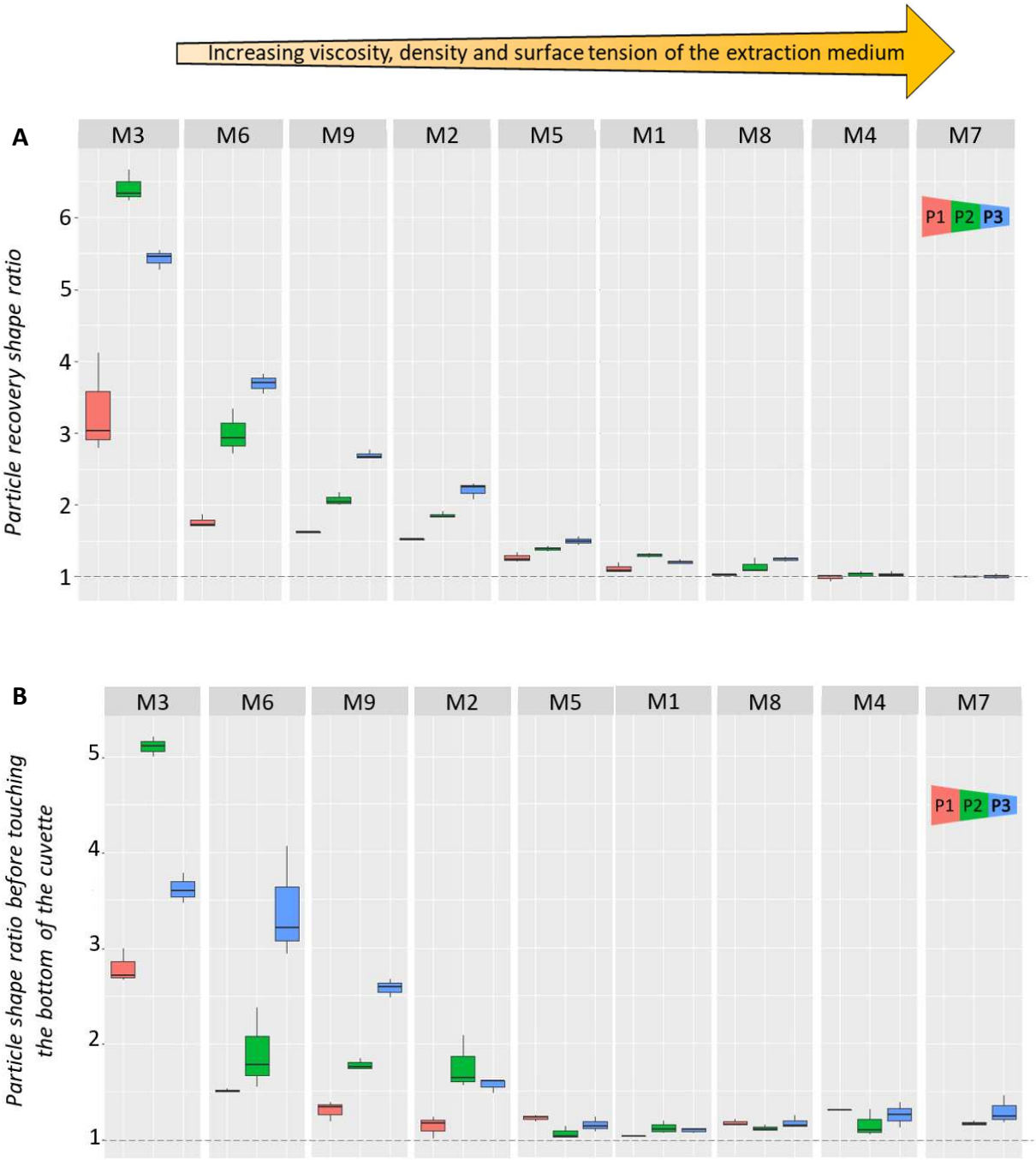

Figure 5. Particle shape ratio corresponding to different extraction media (M1 to M9) and polymer solution (P1, P2 and P3) characteristics. The viscosity and density of the polymer solution decreased from P1 to P3. (A) Particle recovery shape ratio, (B) particle redeformation shape ratio during sedimentation (before touching the bottom of the cuvette), (C) particle length ratio after/before touching the bottom of the cuvette. (For interpretation of the references to color in this figure legend, the reader is referred to the web version of this article).

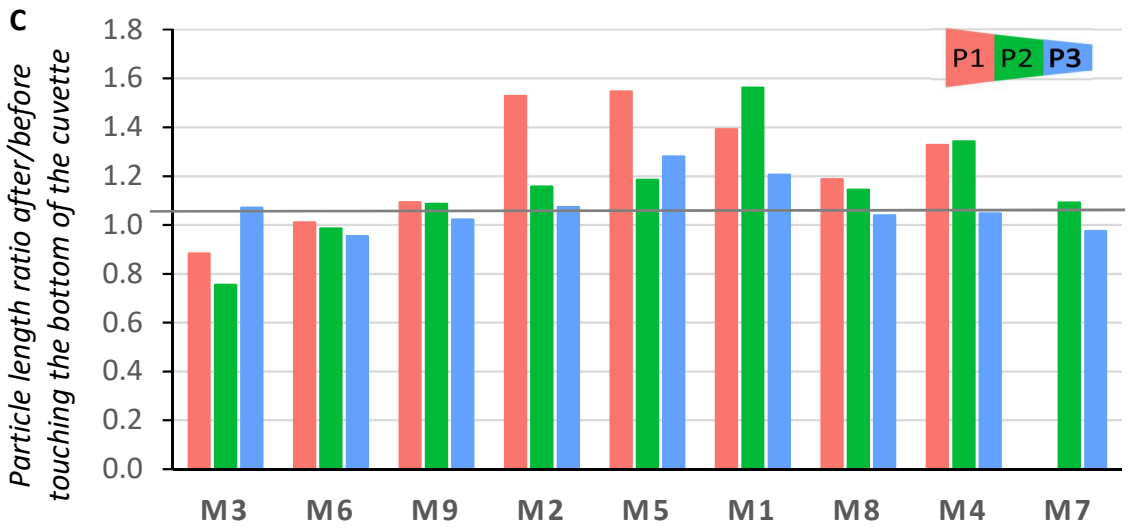

Figure 5 (cont). Particle shape ratio corresponding to different extraction media (M1 to M9) and polymer solution (P1, P2 and P3) characteristics. The viscosity and density of the polymer solution decreased from P1 to P3. (A) Particle recovery shape ratio, (B) particle redeformation shape ratio during sedimentation (before touching the bottom of the cuvette), (C) particle length ratio after/before touching the bottom of the cuvette. (For interpretation of the references to color in this figure legend, the reader is referred to the web version of this article)

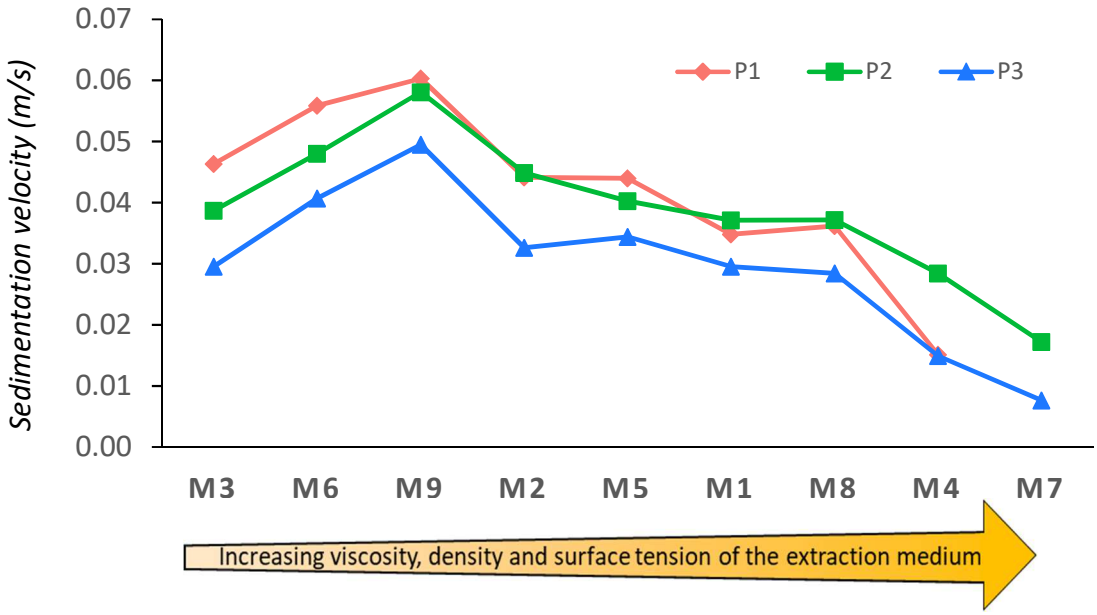

Figure 6. Sedimentation velocity of particles in the extraction media. The viscosity and density of the polymer solution decreased from P1 to P3. (For interpretation of the references to color in this figure legend, the reader is referred to the web version of this article)

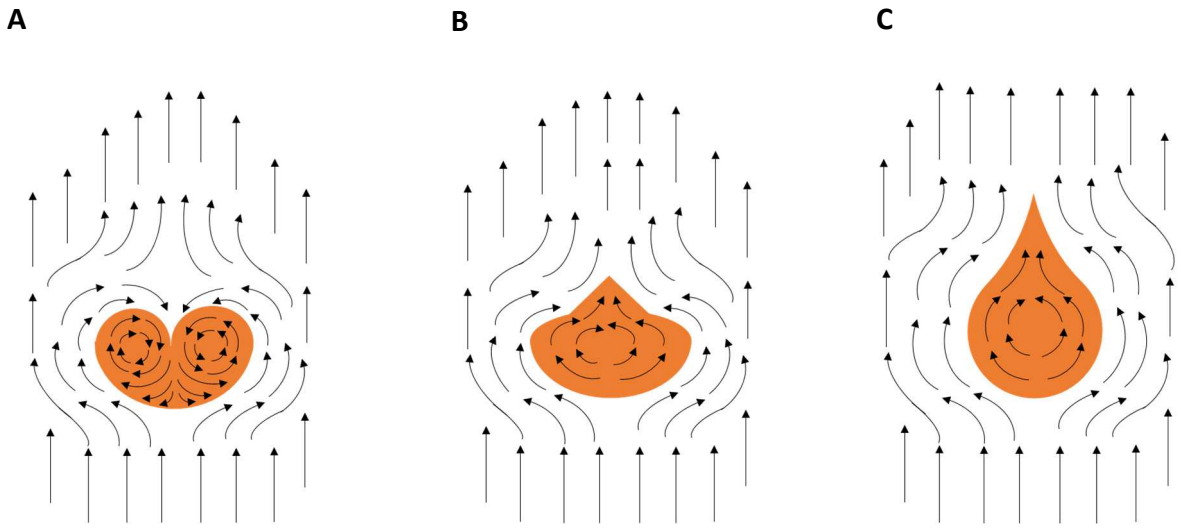

Figure 7. Forces acting on droplets during penetrating a liquid surface. The flow of liquid is (A) turbulent, (B) a combination of turbulent and laminar, (C) laminar.

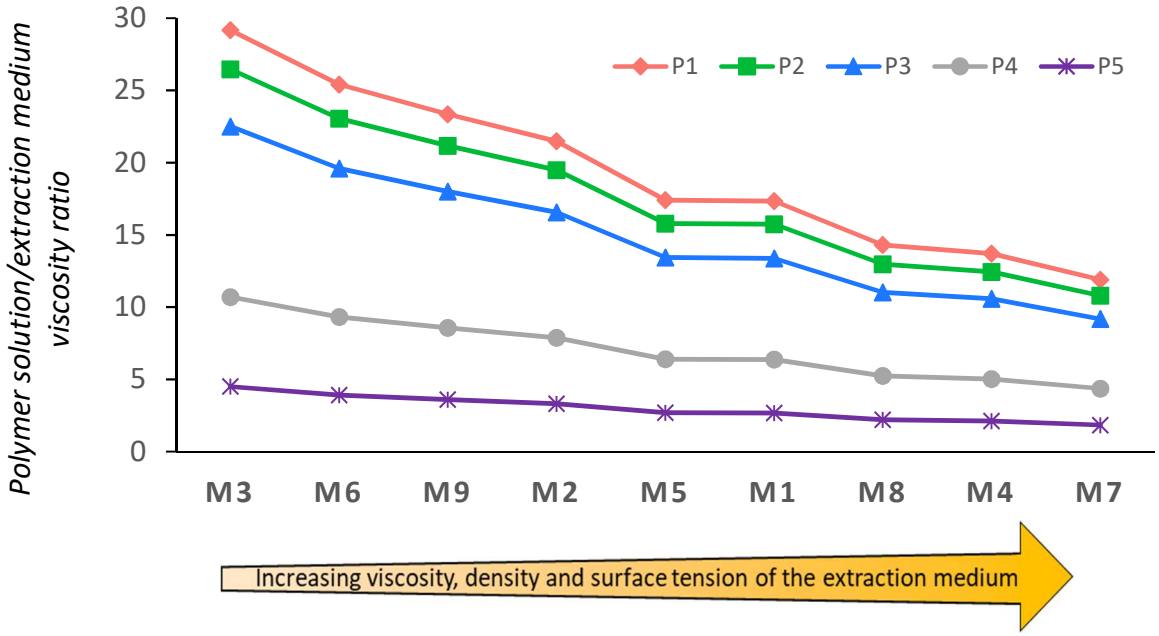

Figure 8. Polymer solution/extraction medium viscosity ratio. (For interpretation of the references to color in this figure legend, the reader is referred to the web version of this article)

Tables

Table 1. Properties of the polymer solutions.

Code name	Polymer conc. (mg/mL)	DMSO (% v/v)	Ethyl acetate (% v/v)	Acetone (% v/v)	Viscosity (mPa.s, 20°C)	Density (g/cm^3, RT)	Surface tension (mN/m, RT)
P1	110	25	75	0	43.18 ± 0.43	0.975 ± 0.003	24.74 ± 0.14
P2	110	25	50	25	39.18 ± 0.59	0.936 ± 0.006	25.01 ± 0.05
P3	110	25	12.5	62.5	33.31 ± 0.56	0.878 ± 0.020	24.52 ± 0.03
P4	80	25	12.5	62.5	15.83 ± 0.33	0.865 ± 0.130	25.53 ± 0.06
P5	50	25	12.5	62.5	6.66 ± 0.32	0.857 ± 0.006	26.64 ± 0.03

Table 2. Properties of the extraction media.

Code name	Ethyl acetate (%v/v)	Ethanol (%v/v)	Water (%v/v)	Viscosity (mPa.s, 20°C)	Density (g/cm^3, RT)	Surface tension (mN/m, RT)
M1	25	50	25	2.49 ± 0.05	0.873 ± 0.000	24.67 ± 0.20
M2	25	62.5	12.5	2.01 ± 0.03	0.848 ± 0.000	23.97 ± 0.02
M3	25	75	0	1.48 ± 0.03	0.803 ± 0.001	21.24 ± 0.16
M4	12.5	50	37.5	3.15 ± 0.17	0.902 ± 0.002	26.22 ± 0.20
M5	12.5	68.75	18.75	2.48 ± 0.07	0.852 ± 0.000	24.34 ± 0.38
M6	12.5	87.5	0	1.70 ± 0.10	0.795 ± 0.001	21.65 ± 0.07
M7	0	50	50	3.63 ± 0.19	0.924 ± 0.001	28.36 ± 0.07
M8	0	75	25	3.02 ± 0.10	0.861 ± 0.001	25.46 ± 0.02
M9	0	100	0	1.85 ± 0.03	0.780 ± 0.001	22.17 ± 0.02

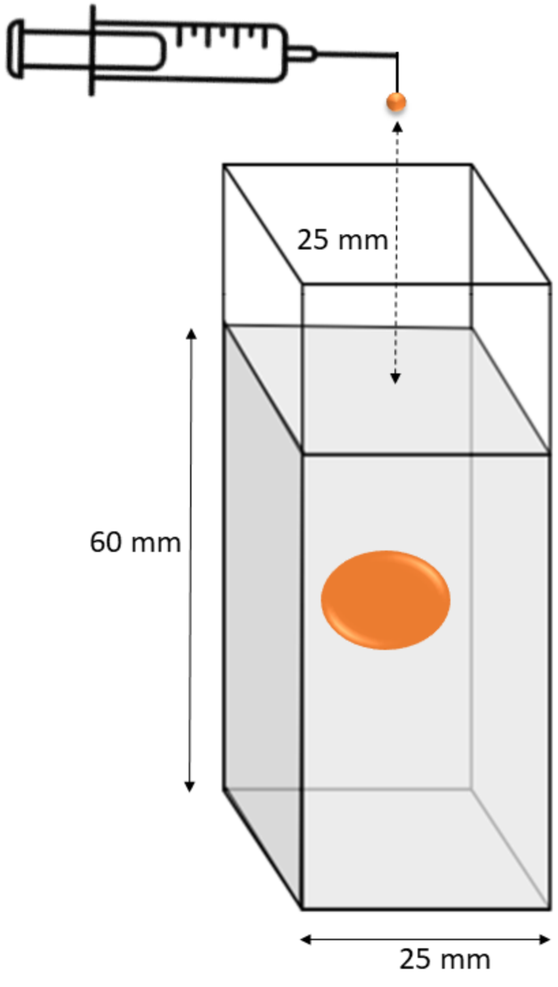
25 mm
60 mm
25 mm